AADE-05-NTCE-75

Influence of the back and side rake angles in rock cutting.

Christophe Coudyzer (Faculté Polytechnique, Mons – Belgium)
Thomas Richard (Diamant Drilling Services, Fleurus – Belgium)

Abstract

In the present research, a testing program was undertaken to investigate the influence of the cutter inclination on both the magnitude and orientation of the cutting force mobilized on the cutter while "scratching" a rock surface.

It is shown that the magnitude of the force is strongly affected by the back rake angle θ while the side rake angle α has barely any effect. The results also demonstrate that the force inclination ψ with respect to the normal to the cutting face varies strongly with the cutter orientation (θ, α) indicating that ψ cannot be viewed as a simple interfacial friction angle as commonly accepted in the literature.

One explanation relies on the presence of a build-up edge of crushed material on the cutting face which controls the flow of failed material in such a way that the angle between the force F and velocity v vectors is almost unaffected.

Introduction

It is generally accepted in the literature that the magnitude of the cutting force acting on a cutter while tracing a groove on the surface of a rock sample is affected by the back rake angle θ (angle between the velocity vector and the normal to the cutter face projected in a plane normal to the rock free surface). This assertion is confirmed by experimental results (Nishimatsu, 1972; Richard, 1999) and commonly explained by Merchant-type solutions (Merchant, 1945; Sellami et al. 1989; Challamel, 1998) assuming (i) a simple plastic flow mechanism with (ii) a unidirectional frictional contact between the material and the cutting face, and (iii) a single failure plane characterized by a Mohr-Coulomb type relationship.

It has been also recognized that the back rake angle affects drastically the angle ψ between the normal to the cutter face and the force vector indicating that ψ is not a measure of the interfacial friction angle between the rock and the cutter face as it is often considered in the literature. These results suggest that a more complex failure mechanism must be considered involving multidirectional frictional contact (Huang *et al*., 1999).

However, to our knowledge there is no report in the literature on the effect of side rake angle (angle between the velocity vector and the normal to the cutter face projected in a plane parallel to the rock free surface) on the magnitude and inclination of the cutting force.

In this research, rock cutting experiments were conducted at the "Faculté Polytechnique de Mons" to precisely measure the effect of both the back and the side rake angles on the magnitude and inclination of the cutting force vector.

All the parameters and variables set or measured during the tests are first introduced. The experimental setup is then presented. Particular attention is given to the experimental procedure. Results are finally presented and discussed.

Nomenclature

Cutting tests were performed at constant cutting speed v under imposed depth of cut d on the free surface of a rock sample.

Tests were conducted with a sharp circular cutter of diameter w = 19 mm. A cutter is considered sharp when the length λ of the edge defect (orthogonal to the cutting edge) remains below 5 microns.

A reference trihedron (s, t, n) is associated with the cutter. The vector, n, is vertical oriented down; the vector s is co-linear to the velocity vector v, and the vector t completes the trihedron($t = n \times s$).

The cutter position within the trihedron is defined by two angles (see Figure 1):

- the back-rake angle θ, defined as the angle between the velocity vector v and the projection k_{sn} of the normal k to the cutter face in the plane defined by the pair (s, n), and
- the side rake angle α defined as the angle between the velocity vector, v and the projection k_{st} of the normal k to the cutter face in the plane defined by the pair (s, t).

We decompose the force vector F (we consider the force applied by the cutter onto the rock) by a projection on the reference trihedron into three components:

- tangential F_s,
- transversal F_t, and
- normal F_n.

The orientation of the force is defined by the angle ψ

between the force vector F and the normal k of the cutter. We also define (see Figure 2):

- ψ_n the angle between the force vector and the projection of the normal to the cutter in the plane (s, n) , and
- ψ_t the angle between the force vector and the projection of the normal to the cutter in the plane (s, t).

Experimental setup

The tests presented in this report were conducted with the Rock Strength Device (Richard *et. al.*, 1998), developed at the University of Minnesota (Figure 3). It comprises a frame with moving parts, a load sensor, a stepper motor, a data acquisition system and a motor indexer connected to a computer.

The main components of the frame are: a traverse with a sample holder (indexed 1 on Figure 3), a moving cart (2) housing the vertical positioning system (3), the load cell (4), and the cutting element holder (5). The horizontal movement of the cart is operated by a computer controlled stepper-motor (6) driving a horizontal motion Archimedes screw (7) via a gearbox (8). The cutting velocity can be set from 0.1 to 8 mm/s, typically 4 mm/s.

The depth of cut is adjusted manually with the vertical positioning system (9). A micrometer (10) indicates the depth of cut, and a locking system (11) permits to block the vertical traveling mechanism against the frame, in order to maintain a constant depth of cut while cutting.

A cutter holder (see Figure 4) was designed to impose independently the back rake θ [0^o, 5^o, 10^o, ...50^o] and side rake angle [0^o, 5^o, 10^o, ...60^o] without affecting the position of the lowest point of the cutter edge. In other words, the two axes of rotation (horizontal for θ and vertical for α) pass through the origin O of the trihedron.

The levering arm caused by the height of the cutter holder is responsible for some cross-talk between the three channels of the piezo-electric three axis load sensor. The sensor was thus fully calibrated with the cutter holder mounted on it and a force being applied at the tip of the cutter.

Experimental procedure

The test procedure consists in tracing a groove at constant depth of cut d on the planned surface of a rock sample. The nominal depth of cut is adjusted with respect to the free surface in three steps:

a. the cutter is moved up to tangency between the cutting edge and the free surface of the rock,
b. the micrometer is initialized to the zero value (the free surface becomes a reference surface) and
c. the depth of cut is adjusted with respect to the «zero».

Several tests (test series) can be conducted on the same planned surface at different depths of cut, and thus different cross-section areas. Meeting the tangency precisely is not an easy task and is usually a source of imprecision. Therefore, after a test series has been completed, the depth of each groove (or effective depth of cut, d_e) traced on the sample surface can be "controlled" on 4 or 5 points along the groove with a mechanical micrometer.

A test series consists of a succession of ten cutting tests performed at depth of cut ranging from 0.1 to 1 mm with a step of 0.1 mm between two successive tests. The "sharpness" of the cutter edge was controlled between every test series with a microscope.

Rock materials

Most of the cutting tests were conducted in samples of Lens limestone. This material was selected for its high homogeneity and medium strength. The homogeneity of the material and the features of the cutting test guarantee a sufficiently low dispersion in the measurements. The medium strength (uniaxial compressive strength, q = 30 MPa) ensures that the cutting process will be dominated by the ductile regime (plastic flow ahead of the cutter) and that brittle failure, (chipping characterized by macroscopic cracks) is negligible. Additional tests were conducted in Vosges sandstone. Some mechanical properties of these materials are summarized in Table 1.

Experimental program

A set of 25 geometrical configurations (one configuration corresponds to one pair (θ, α)) was selected and a test series was conducted for each configuration on samples of Lens limestone. For some configurations, the full tests series could not be completed (magnitude of forces above the sensor limits).

During each test, the three components (F_s, F_n, F_t) of the cutting force are recorded (at a sampling rate of 25 samples per mm). For some of the tests series, the effective depth of cut was measured with a micrometer in order to precisely estimate the cross-section area A_c of the groove and to compute the specific energy.

At large side rake angle ($\alpha > 30^o$) and low back rake angle ($\alpha < 30^o$), the cylindrical carbide body of the cutter was in contact with the groove bottom above a critical depth of cut; the results pertaining to these tests were disregarded in the analysis.

Analysis of experimental results

After a test has been run an average value of each force component is taken over a representative section, see Figure 5 (in the sequel, the term "force component" or the symbol associated to the term refers to the averaged value).

As illustrated in the example shown in Figure 6, the three

force components increase "almost" linearly with the cross-section area of the groove being traced. We write

$$F_s = \varepsilon A_c, \quad F_n = \zeta_n F_s, \quad F_t = \zeta_t F_s \quad (1.1)$$

with

$$\zeta_n = \tan(\psi_n + \theta), \quad \zeta_t = \tan(\alpha - \psi_t) \quad (1.2)$$

The specific energy ε (energy required to cut a unique volume of rock) is estimated for each test series as the slope of the best linear fit run over the set (A_c, F_s)[1].

The two angles ψ_n and ψ_t are computed according to (1.2) from the best linear fit run over the sets (F_s, F_n) and (F_s, F_t), respectively.

Force inclination

We draw two main observations from the test results (see Figure 7):

1. The angle ψ_n is strongly affected by the back rake angle θ but almost unaffected by the side rake angle α.
2. Similarly, the angle ψ_t is strongly affected by the side rake angle α but almost unaffected by the back rake angle θ.

These results provide evidence that (i) ψ can not be interpreted as a measure of the interfacial friction angle between the rock material and the cutter face, and (ii) ψ is not controlled by a unidirectional flow of material along the cutting face.

Moreover, while ψ_n and ψ_t vary "rapidly" with θ and α respectively, the angles $\theta+\psi_n$ and $\alpha-\psi_t$ vary "slowly" with θ and/or α (Figure 8). The tangential component of the force does increase with the side rake angle but remains small compared to the two other components, so that the force vector rotates only slightly out of plane (n, s) with increasing side rake angle.

In others words, the orientation of the force vector in the referential (s, t, n) is only slightly affected by the orientation of the normal to the cutter face (for a fixed cutter velocity). As an illustration, the angle ψ_v between the force F and velocity v vectors can be considered as independent of the magnitude of the back and side rake angles as illustrated in Figure 9 (with increasing side rake angle, the vector F rotates out of plane (n, s) around the vector v).

One explanation invokes the presence of a wedge of dead material sticking to the cutter face; this wedge divides the flow of material into upward, backward and transverse flows. Varying the back and side rake angles affects the geometry of the wedge resulting in the increase of one flow direction at the expense of another one, which in turn affects the orientation of the force vector with respect to the normal but maintains a constant angle between F and v. Illustrative drawings of two different cases are shown in Figure 10.

One limiting case ($\theta = 90^o$) corresponds to the case of the cutting face moving along the rock free surface, which is equivalent to the case of a wear flat. It is interesting to notice that the point deduced from tests conducted with a blunt cutter (inclination of the force mobilized across the wear flat) aligns well in the (θ, ψ_n) diagram with the points pertaining to tests conducted with sharp cutter, see Figure 11 ($\alpha = 0^o$). As clearly demonstrated in this figure, ψ_n varies between two apparent limits, i.e. $\psi_n = 33^o$ for $\theta = 5^o$ and $\psi_n = -32^o$ for $\theta = 90^o$. There are some experimental evidences (Detournay and Defourny, 1992; Adachi *et. al.*,1996; Lhomme, 1999) indicating that the friction coefficient measured across the wear-flat/rock interface is well correlated to the material internal friction angle.

Based on these observations, it is thus legitimate to suggest that the angle ψ_n (ψ) is mainly controlled by rock properties and almost independent of the frictional properties of the tool cutting face. Dagrain (2003) draws similar conclusions from comparative tests conducted with standard and "polished" cutter (the cutting face had polished finish).

Force amplitude

As commonly reported in the literature, the specific energy increases with the back rake angle, see Figure 12. This increase is certainly associated with the increase of the "backward flow" at the expense of the "upward flow". The upward plastic flow can be viewed as uncontained while the backward flow is contained resulting in higher force magnitude due to the dilatant nature of the rock material.

At the same time, we observe that a variation of the side rake angle between 0 and 45^o does not affect the measured specific energy, see Figure 13.

Conclusions

This paper reports results of rock cutting tests performed with sharp cutters (no chamfer) at various back and side rake angles. These results confirm that the angle between the force vector and the normal to the cutter face can not be taken as a measure of the interfacial friction angle between the rock and the cutter face. Furthermore, the results indicate that the angle ψ_v between the force and the velocity vectors is almost a constant independent of the cutter inclination.

Similar tests and analysis are being extended to standard chamfered cutters. These results have practical implication in terms of bit design; properly selecting back and side rake angles can affect the bit drilling efficiency and steerability.

Acknowledgments

The authors are very grateful to Abdelhakim Hahati for his help creating the drawings and very thankful to

[1] The force component F_s is the only component with a non-zero work.

Sebastian Desmette, Emmanuel Detournay, Fabrice Dagrain and Jean-Pierre Tshibangu for many useful discussions.
We would like also to express our gratitude to the Region Wallone for financing this research and approving this publication.

Nomenclature

θ = *back rake angle (°)*
α = *side rake angle (°)*
ψ = *force inclination (°)*
ψ_t ψ_n = *projection of ψ in planes (s,t) and (n,s)*
ψ_v = *angle between the force and velocity vectors*
F = *cutting force vector*
$F_{s,n,t}$ = *force vector components*
v = *velocity vector*
k = *normal to the cutter face*
d = *depth of cut (mm)*
A_c = *cross sectional area of the groove (mm^2)*
ε = *specific energy (MPa)*
w = *cutter diameter (mm)*
λ = *cutting edge defect length (mm)*
q = *uniaxial compressive strength (MPa)*

References

1. Nishimatsu, Y.: “The mechanics of rock cutting”, *Int. J. Rock Mech. Min. Sci.* v. 9, 1972.
2. Richard, T.: “Determination of rock strength from cutting tests”, Master Thesis, University of Minnesota, 1999.
3. Richard, T., Detournay, E., Drescher, A., Nicodeme, P., Fourmaintraux, D.: “The scratch test as a means to measure strength of sedimentary rocks”, *In SPE Proceedings Eurock Trondheim 98,* SPE 47196, 1998.
4. Merchant, M.: “Basic mechanics of the metal cutting process”, *Journal of Applied Mechanics* 11, A168-A175, 1944.
5. Sellami, H., Fairhurst, C., Deliac E., and Delbast, B.: “The role of in-situ rock stresses and mud pressure on the penetration rate of PDC bits”, In V. Maury and D. Fourmaintraux (Eds.), *Rock at Great Depth*, pp 769-777, Balkema, 1989.
6. Challamel, N.: “Application of yield design for understanding rock cutting mechanisms”, *In SPE Proceedings Eurock Trondheim 98,* SPE 47340, 1998.
7. Huang, H., Detournay, E. and Belier, B. “Discrete element of modeling of rock cutting”, *In proceedings of the North American Rock Mechanics Symposium*, Narms99, held in Vail, 1999.
8. Detournay, E. and Defourny, P.: “A phenomenological model for the drilling action of drag bits”, *Int. J. Rock Mech. Min. Sci* 29, 1 pp 13-23, 1992.
9. Lhomme T.: “Frictional contact at rock tool interface, an experimental study”, Master Thesis University of Minnesota, 1999.
10. Adachi, J., Detournay, E., and Drescher A.: “Determination of rock strength parameters from cutting tests”, In F. Aubertin and H. Mitri (Eds.), *Rock Mechanics, Tools and Techniques, Proc. 2nd North American Symposium of Rock Mechanics*, Montreal, **2**, pp. 1517-1523.
11. Dagrain, F., Richard, T., Detournay, E.: “Effect of the Polishing of a Cutter on the Cutting Effciency”, *North American Rock Mechanics Symposium*, 2002.
12. Dagrain, F.: “Personal communication”, 2004.

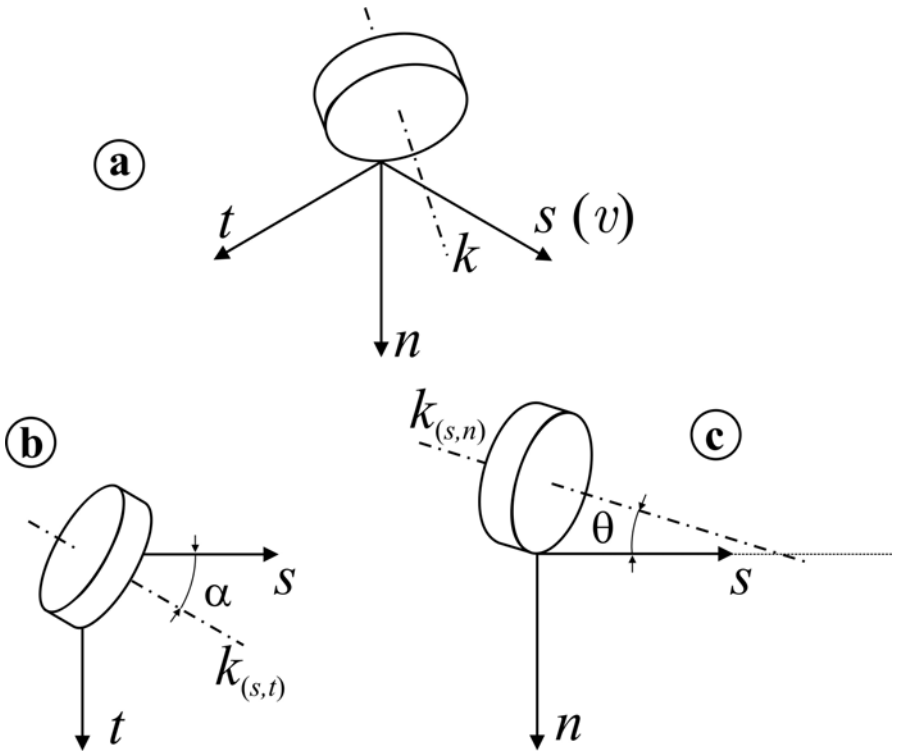

Figure 1: (a) Three dimensional view of a cutter with normal *k* in the referential (*s, t, n*), the velocity vector *v* is aligned with *s*. (b) Projection in the plane (*s, t*) and definition of the side rake angle, α. (c) Projection in the plane (*s, n*) and definition of the back rake angle, θ.

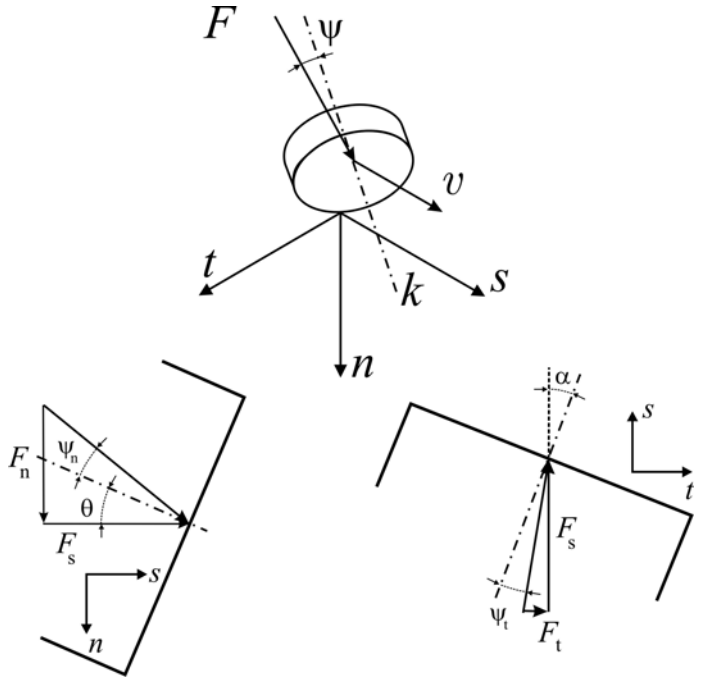

Figure 2: Definition of the angle ψ. Projection ψ_n and ψ_t in the planes (*s, n*) and (*s, t*), respectively.

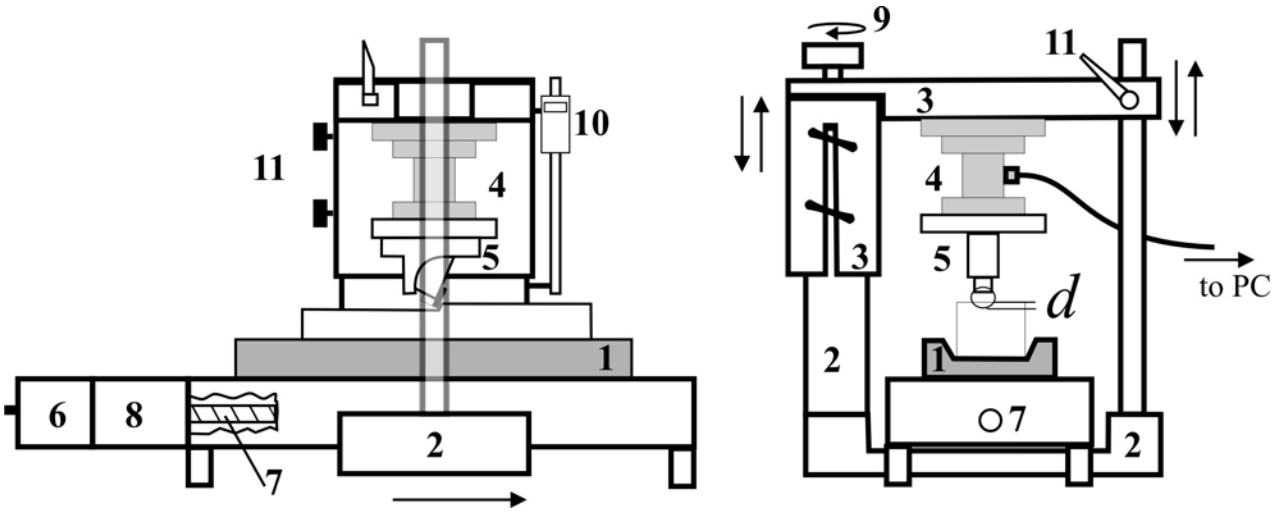

Figure 3: Sketch of the Rock Strength Device.

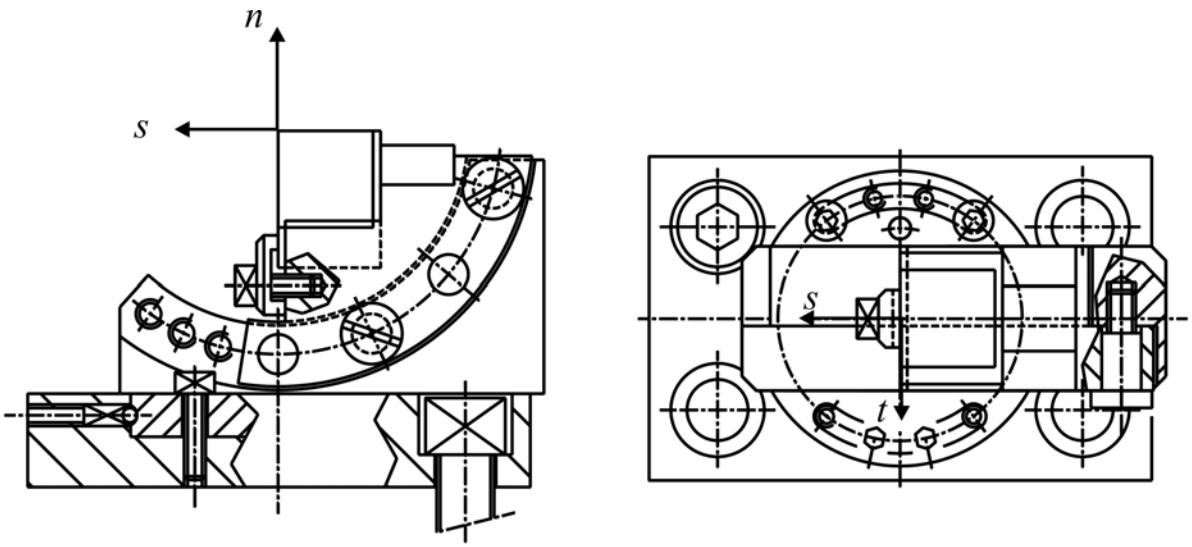

Figure 4: Drawings of the cutter holder with adjustable back and side rake angles. Side and top view of the cutter holder, after Marc Radermaecker and Abdelhakim Hahati, 2002.

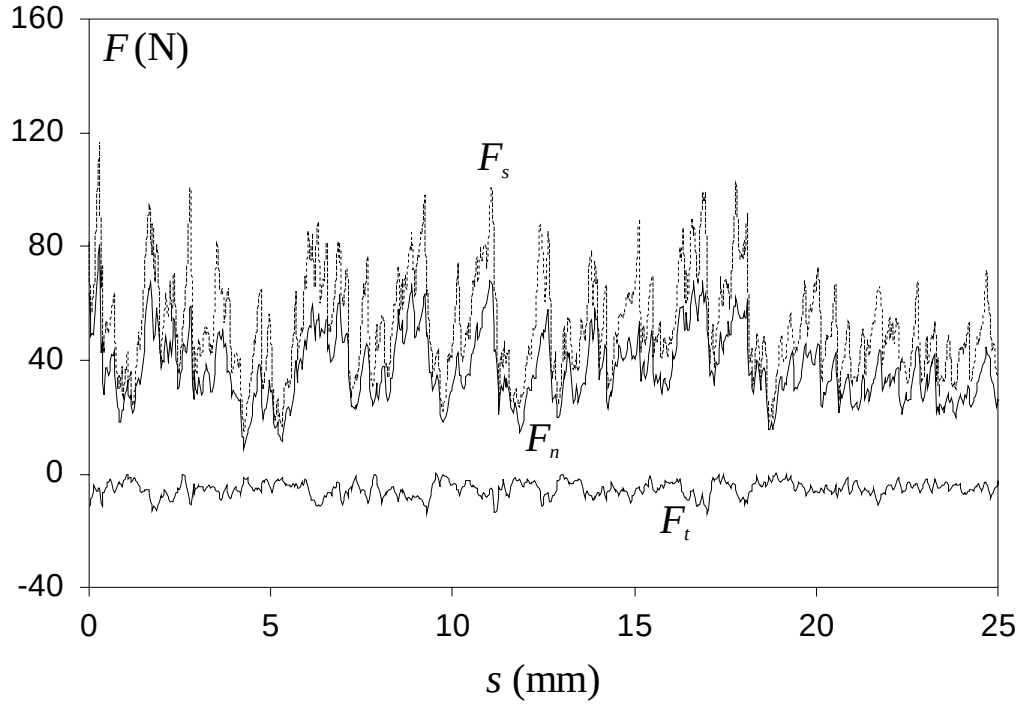

Figure 5: Example of the force components signal (θ = 15°, α = 20°), Lens limestone (the tangential component is shown negative for the sake of clarity).

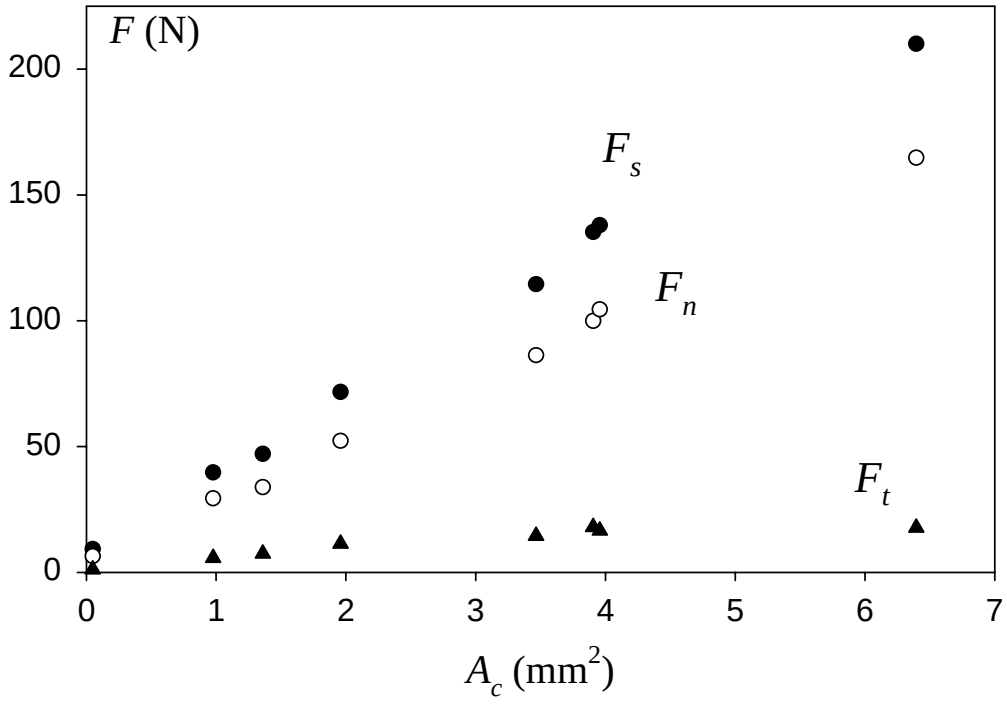

Figure 6: Evolution of the three force components with the cross-sectional area (Lens limestone, θ = 15°, α = 30°).

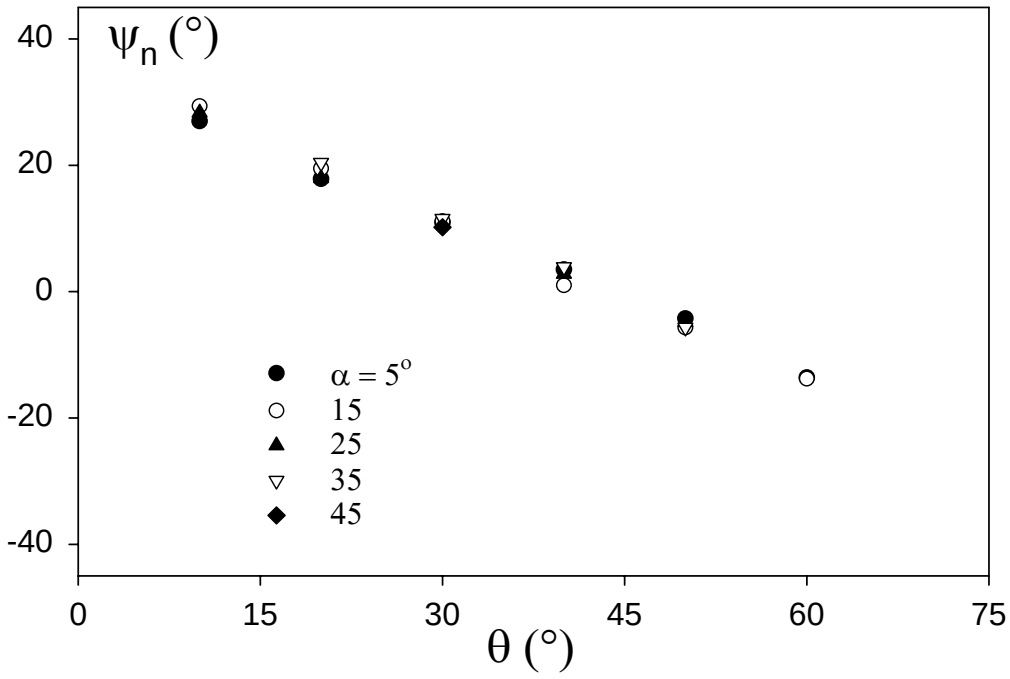

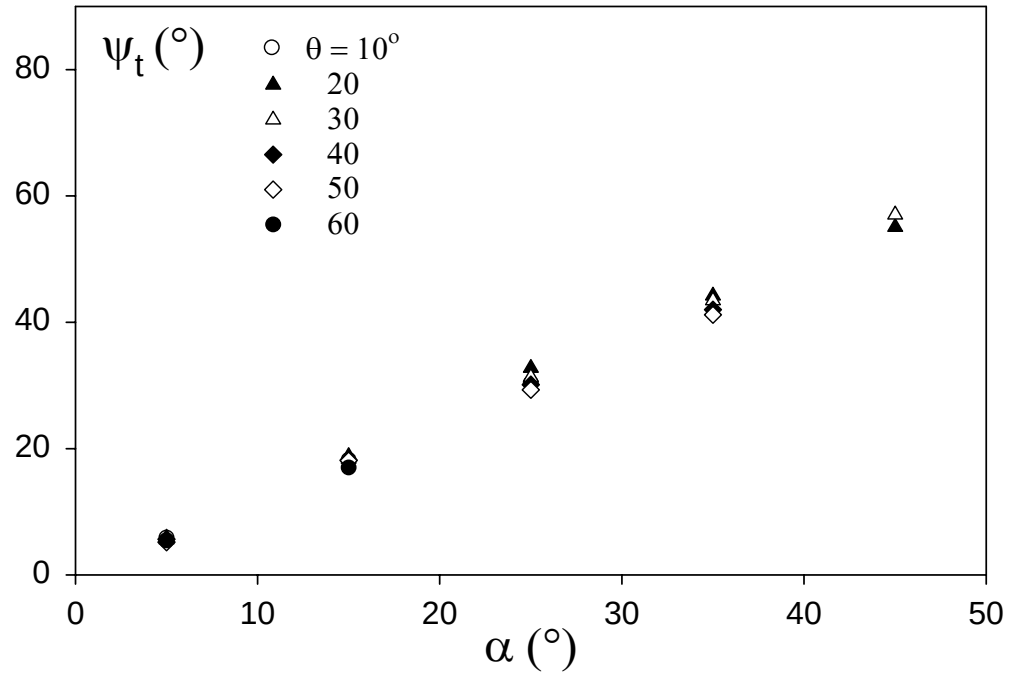

Figure 7: Evolution of ψ_n and ψ_t with θ and α (Lens limestone).

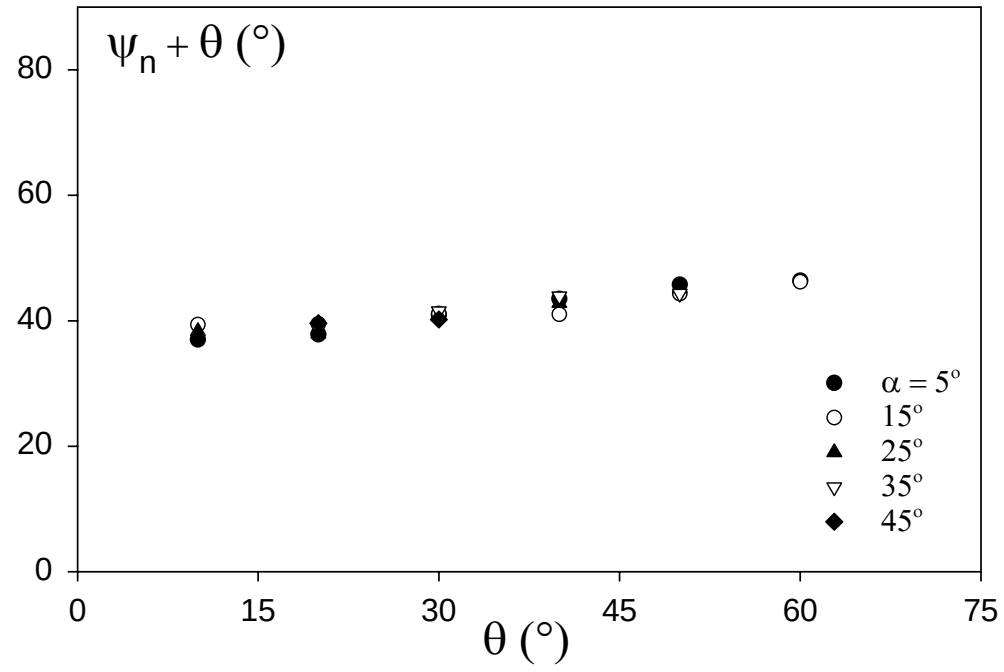

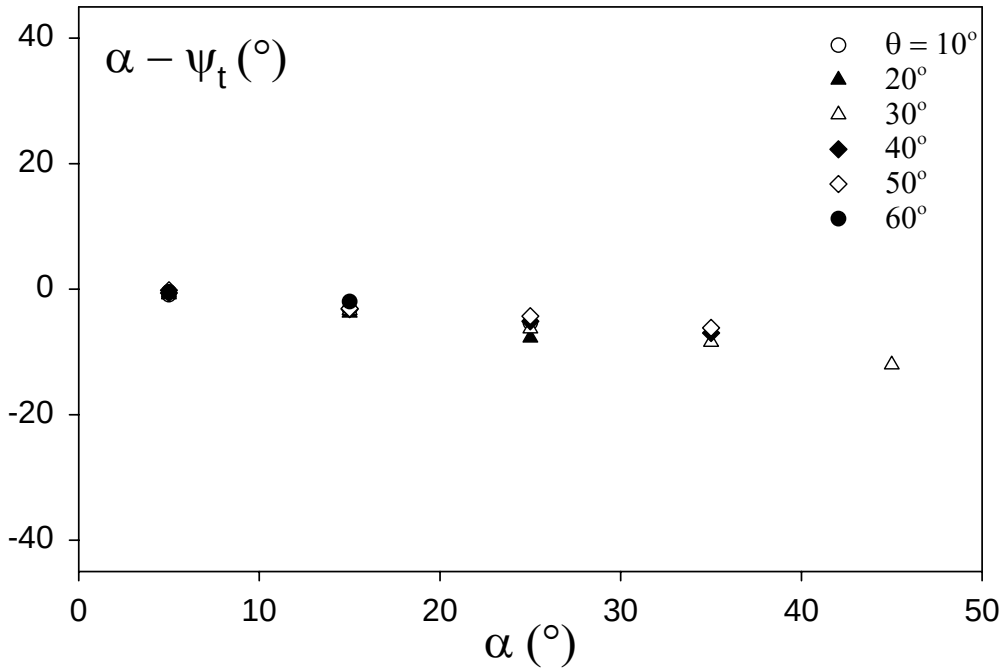

Figure 8: Evolution of $\psi_n+\theta$ and $\alpha-\psi_t$ with θ and α (Lens limestone).

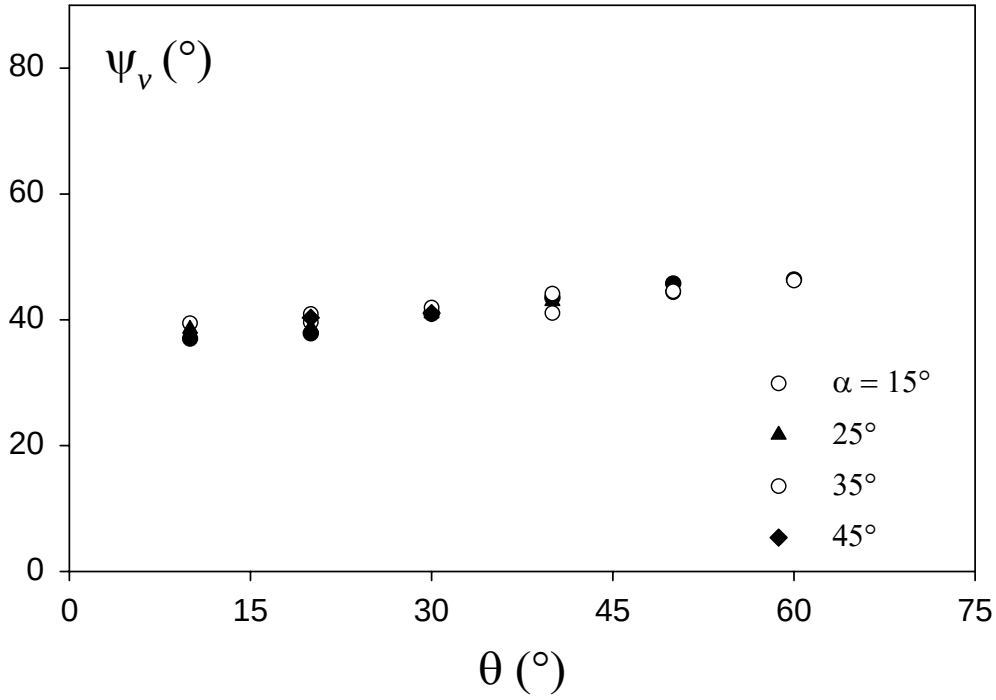

Figure 9: Evolution of ψ_v with θ and α (Lens limestone).

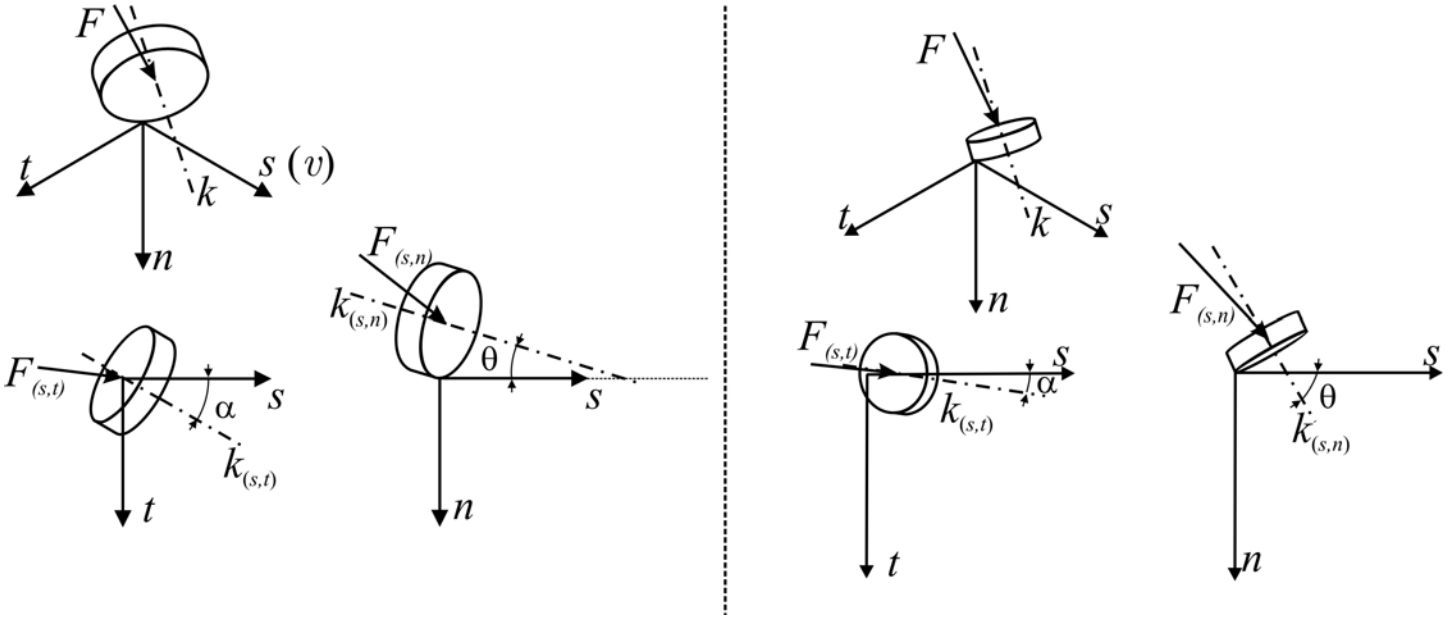

Figure 10: 3D sketch for two different cases: 1. θ =15° α =30° and 2. θ =60° α =5°

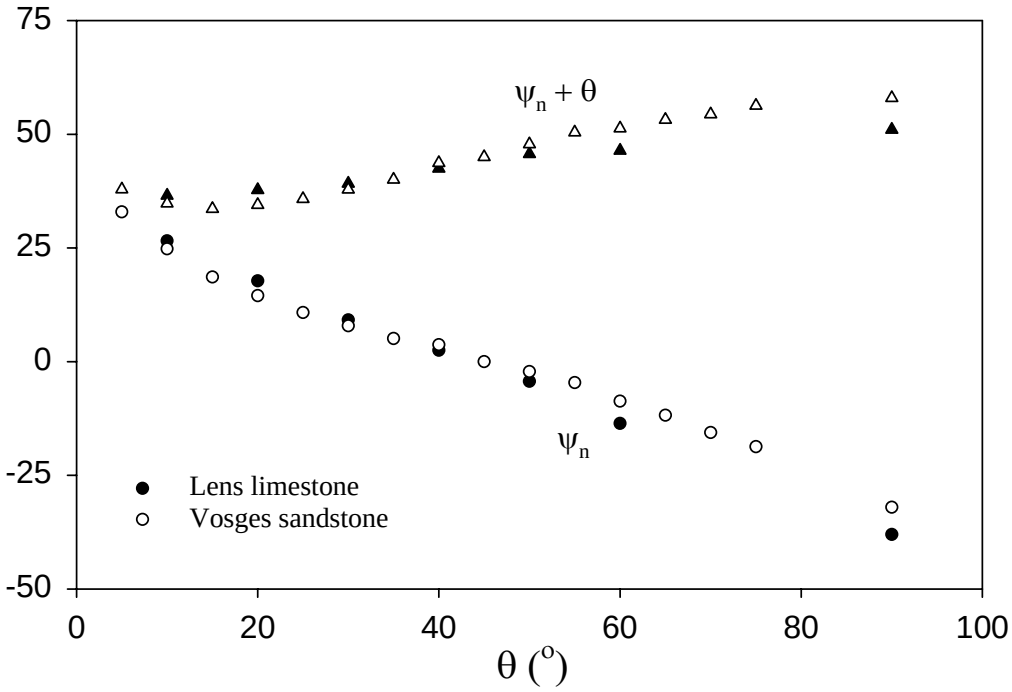

Figure 11: Evolution of the angles ψ_n and $\psi_n + \theta$ with θ ($\alpha = 0^o$). Tests conducted in Lens limestone and Vosges sandstone.

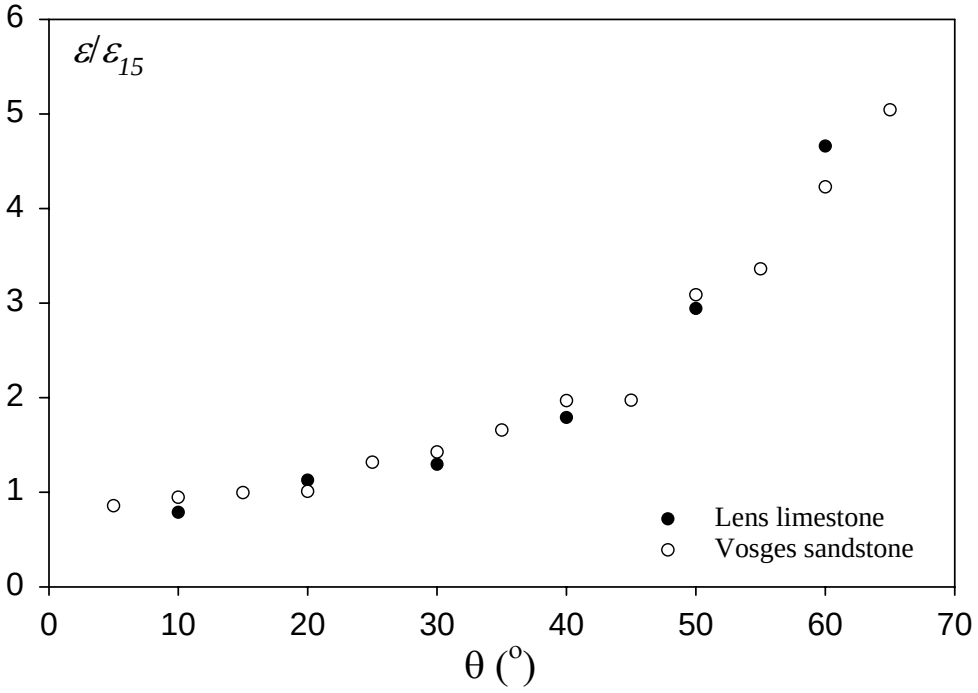

Figure 12: Evolution of the specific energy (scaled with the specific energy measured at $\theta = 15^o$). Data for the Vosges sandstone are extracted from Richard, 1999.

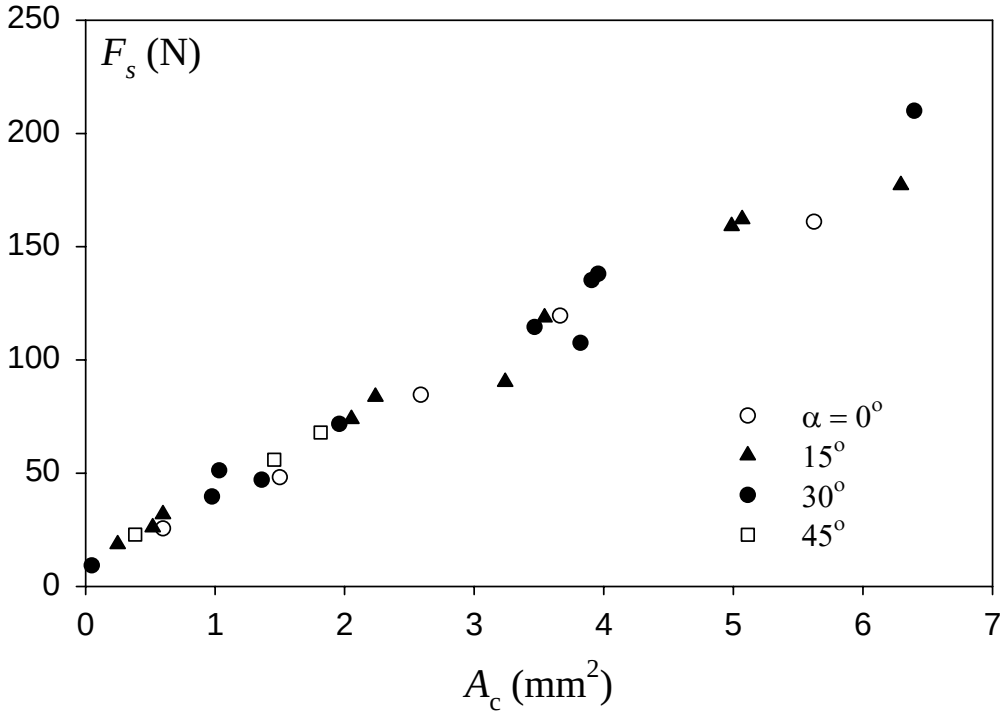

Figure 13: Evolution of the tangential force component F_s with A_c for three different side rake angles (θ = 15°).

	Lens	Vosges
***Y* (MPa)**	1700	5300
***q* (MPa)**	30	16
***T* (MPa)**	3.27	1.25
φ (°)	38.4	34.3
***C* (MPa)**	7.5	2.65
Average grain size (μm)	50	150

Table 1: Rock properties (after Dagrain, 2004).
(Young's Modulus, *Y*; uniaxial compressive strength, *q*; tensile strength, *T* ; internal friction angle, ϕ and cohesion).